ACS APPLIED MATERIALS & INTERFACES

Research Article

www.acsami.org

Fabrication of Large Domain Crack-Free Colloidal Crystal Heterostructures with Superposition Bandgaps Using Hydrophobic Polystyrene Spheres

Zhongyu Cai,[†] Yan Jun Liu,[‡] Jinghua Teng,*[,‡] and Xianmao Lu*[,†]

[†]Department of Chemical and Biomolecular Engineering, National University of Singapore, 4 Engineering Drive 4, Singapore 117576

[‡]Institute of Materials Research and Engineering, Agency for Science, Technology and Research (A*STAR), 3 Research Link, Singapore 117602

Supporting Information

ABSTRACT: An improved convective self-assembly method was developed to fabricate crack-free colloidal crystal heterostructure over a relatively large area. A composite opaline heterostructure composed of polystyrene (PS) colloids was first fabricated. Subsequent calcination of the opaline heterostructure led to the formation of inverse opaline heterostructure composed of SiO_2 or TiO_2. Both opaline and inverse opaline heterostructures demonstrated long-range ordering in a relatively large domain (>100 × 100 μm^2). Optical reflection measurements of the inverse opaline heterostructures showed dual stop bands as a consequence of the superposition of the stop bands from the individual compositional colloidal crystals (CCs). In addition, the relative position of the two stop bands can be adjusted by varying the size of the colloidal spheres in the original CCs template. Both types of colloidal crystal heterostructures can be used for optical filters, high-efficiency back-reflectors or electrodes in solar cells, differential drug release, and protein patterning.

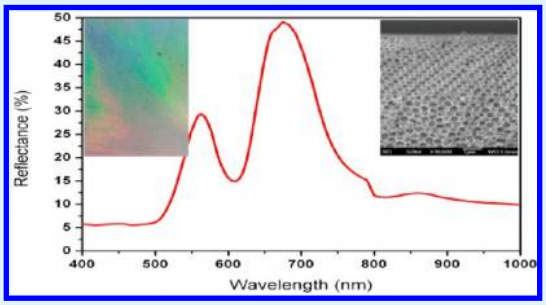

KEYWORDS: *colloidal crystals, heterostructure, convective self-assembly, large area, crack-free, superposition stop bands*

1. INTRODUCTION

Over the past decade, a variety of techniques, including vertical deposition,[1,2] gravitational sedimentation,[3,4] horizontal deposition,[5−7] physical confinement,[8−10] centrifugation,[11] electrophoretic deposition,[12−14] Langmuir−Blodgett (LB) technique,[15] and floating self-assembly,[16] have been developed to fabricate high-quality colloidal crystals (CCs). Three-dimensional (3D) self-assembled CCs, in particular, have drawn much attention, and their fabrication and characterization have been widely investigated. However, the functionalization of 3D CCs has been reported only until recent years. For instance, artificial defects engineering[17] has been used to create various types of defects, such as point defects, line defects, and planar defects, into 3D CCs for photonic crystal (PhC) application.[17,18] In addition to embedding artificial defects, another way to functionalize 3D CCs is through fabricating heterostructured CCs.[19,20] Recently, heterostructured CCs, including two-layer opaline films,[21,22] sandwich-like CCs,[23,24] and colloidal superlattice,[25] have been successfully fabricated. The photonic band of these structures can be conveniently engineered by changing the lattice constant. The colloidal crystal (CC) heterostructures prepared via these methods are mostly opal structures. In fact, high-quality inverse opaline heterostructures are more desirable owing to their wider applications.[26−28] However, they are more challenging in the fabrication, especially for defect-free single crystals in a relatively large domain using traditional preparation methods.[28,29] For example, LB technique is widely used in the fabrication of CC heterostructures but hard to achieve a full 3D ordering.[30−34]

The convective self-assembly method is another well-known method for the fabrication of opaline heterostructures by sequential deposition of spheres on a substrate[6,21,22,25,35,36] but with limitations. The surface on which the opaline film is deposited should be hydrophilic given that most colloids are dispersed in water. Therefore, in most cases, SiO_2 colloids are used for fabricating opaline heterostructures,[21,22,35] or at least the bottom layer is a hydrophilic SiO_2 opal film.[6] Due to the hydrophobicity, polymer colloids such as polystyrene (PS) and poly (methyl methacrylate) are seldom used to fabricate CC hetrostructures.[36−38] Moreover, polymer colloidal spheres tend to redisperse when a dry CC film is immersed in water. Therefore, a post treatment process such as annealing is often necessary to maintain the crystalline integrity of the as-deposited opal film,[39] leading to change in optical properties. Consequently, the structural and optical properties of its inverse opal replica will also be affected. Yan et al. employed a layer transfer technique combined with flow-controlled vertical deposition to form opaline hetero PhCs using PS colloidal

Received: July 25, 2012
Accepted: October 2, 2012
Published: October 2, 2012

   dx.doi.org/10.1021/am3014482 | ACS Appl. Mater. Interfaces 2012, 4, 5562−5569

Scheme 1. Schematic Illustration for the Fabrication of Crack-Free CC Heterostructure Films

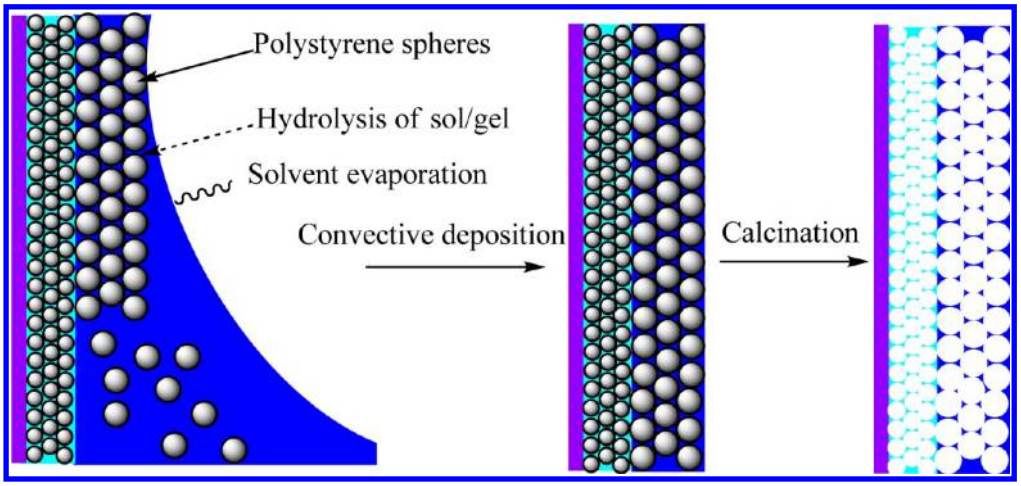

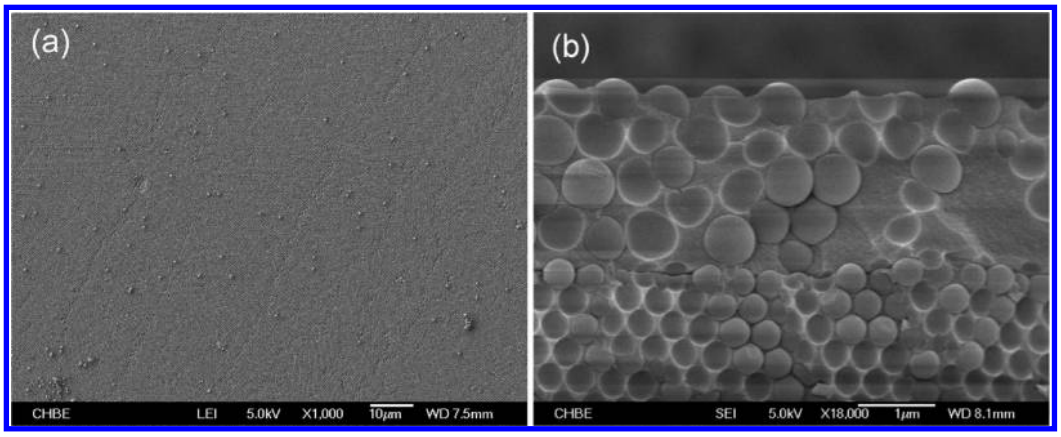

Figure 1. Top and cross-sectional views of PS/SiO_2 composite opaline heterostructure fabricated using 420 and 715 nm PS spheres.

spheres.[40] This technique is also suitable for planar defect engineering in a self-assembled colloidal PhC, but it requires precise control of the film withdrawal when transferring one layer to another and involves multiple steps.

Here, we report a facile fabrication of high-quality CC heterostructures via an improved convective self-assembly method. In this method, a water-soluble organometallic sol–gel was mixed with PS colloids. Then, PS spheres with one size were first deposited on a solid glass substrate as the bottom opaline layer. On top of it, another opaline layer consisting of PS spheres with a different size can be subsequently deposited, forming an opaline heterostructure. Finally, inverse opaline heterostructures were achieved by selectively removing the PS spheres through calcination. Using this method, CC heterostructures composed of either the same material with different pore sizes or different materials (e.g., SiO_2 and TiO_2), regardless of hydrophilic or hydrophobic interface, can be obtained. Compared to conventional methods, large-domain and high-quality heterostructures can be fabricated within a few steps at low cost.

2. EXPERIMENTAL SECTION

2.1. Materials. All chemicals, including styrene (99%, Aldrich), potassium persulfate (99%, Aldrich), ethanol (100%, Aldrich), sulfuric acid (98%, Merck), hydrogen peroxide (35%, Scharlau Chemie S.A.), tetraethyl orthosilicate (TEOS, 98%, Aldrich), titanium(IV)-bis-lactato-bisammonium dihydroxide (TiBALDH, 50% solution, Sigma–Aldrich), and hydrochloric acid (37%, Sigma-Aldrich), were used as purchased. Microscope cover glasses (22 mm × 22 mm × 0.3 mm, Deckgläser) were used as substrate for the fabrication of PS/SiO_2 CCs. The glass substrate was treated in a piranha solution (a mixture containing concentrated 98% sulfuric acid and 35% hydrogen peroxide with a volume ratio of H_2SO_4/H_2O_2 = 3:1 v/v) at 60 °C for 2 h before use. (*Caution*! Piranha and the components of piranha are highly corrosive chemicals that present numerous health hazards. When H_2O_2 and H_2SO_4 are combined, an exothermic, potentially explosive reaction will result. Prior to working with piranha solutions, the reader is encouraged to take all necessary precautions.)

PS spheres were synthesized using an emulsifier-free emulsion polymerization technique.[41] PS spheres with diameters of 350, 420, 435, 495, 560, and 715 nm were used in this study. The size and size distribution of the spheres were obtained from field emission scanning electron microscopy (FESEM) measurements, which showed that the diameters of the PS spheres had a standard deviation of less than 3%.

2.2. Fabrication of Crack-Free PS Opaline and SiO_2 (TiO_2) Inverse Opaline Heterostructures. Scheme 1 schematically demonstrates the procedures for the fabrication of high-quality SiO_2 (or TiO_2) CC heterostructures over a large area. The fabrication was conducted in two steps: (i) convective self-assembly of PS/SiO_2 composite CC films; (ii) calcination of the composite CC films to remove PS spheres. In the first step, PS/TEOS suspensions were used to convectively self-assemble into hybrid CCs. In a typical process, 0.289 mL of a 420 nm PS colloidal suspension (4.330 vol %, purified by centrifugation) was added to a mixture of 10 mL of deionized H_2O and 0.08 mL of hydrolyzed TEOS solution. The TEOS sol consists of TEOS, absolute ethanol, and 0.10 M HCl (1:2:1 ratio by volume). The sol was sonicated for 30 min prior to use. The glass substrates were vertically suspended in a vial containing the colloid/TEOS suspension. The solvent content was evaporated slowly over a period of 30 h at 65

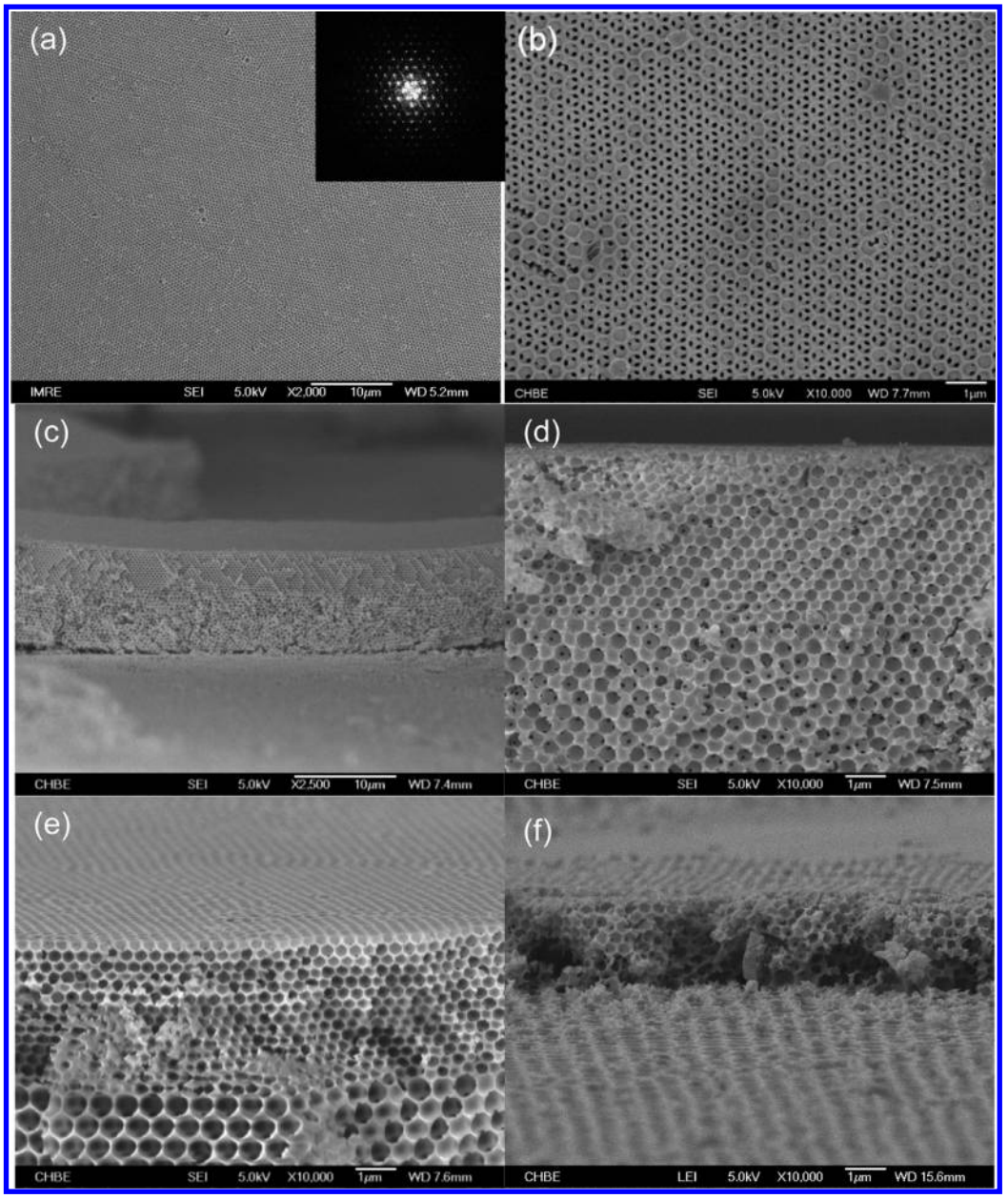

Figure 2. (a,b) Top views of fabricated SiO_2−SiO_2 (560−435 nm) inverse opaline heterostructure films and upper inset showing a FFT of the sample shown in (a); (c,d) cross-sectional views of the SiO_2−SiO_2 (560−435 nm) inverse opaline heterostructure comprising 435 nm air spheres at the top and 560 nm air spheres at the bottom; (e,f) cross-sectional view (e) and (f) the interface formed between 715 and 420 nm SiO_2−SiO_2 inverse opaline heterostructure films.

°C in an oven to allow the deposition of a thin film of PS CCs onto the suspended substrate. Afterward, 0.112 mL of PS colloidal spheres with a different size (715 nm, 6.703 vol %) were grown on top of the bottom layer for 30 h. In the second step, the resulting PS/SiO_2 composite CCs were subsequently calcined in air to obtain SiO_2 inverse opaline heterostructure. The films were calcined in air with a muffle furnace at 450 °C (1 °C/min) for 4 h to completely remove the polymer template and partially sinter the SiO_2 structure.

For the fabrication of TiO_2 inverse opaline heterostructure, the same deposition conditions were applied except that TiBALDH, a water-soluble TiO_2 precursor, was used as a substitute for the TEOS in solution (in molar ratios equivalent to TEOS).

2.3. Characterization. Scanning electron microscope (SEM) images of the PS/SiO_2 CCs and SiO_2 inverse opaline heterostructure were recorded using a JEOL JSM-6700F FESEM. Surface mapping of the samples was also carried out with FESEM system. Optical spectra were obtained on a Shimadzu UV-3600PC UV−vis-near-infrared (UV−vis-NIR) spectrophotometer and a UV−vis-NIR Range Microspectrophotometer (CRAIC QDI 2010).

3. RESULTS AND DISCUSSION

3.1. PS/SiO_2 Opaline Structures. Figure 1 shows the top and cross-sectional SEM images of the PS/SiO_2 composite opaline heterostructure. The PS spheres with two different sizes are relatively ordered in the matrix of SiO_2. The PS/SiO_2 composite films display long-range ordered structure without cracks. This confirms that, with our method, hydrophobic colloidal spheres can be used to fabricate high-quality CC heterostructure without modifying the surface of the PS spheres with surfactant.[40] The obtained PS/SiO_2 opaline heterostructure can be further used for the fabrication of either PS opaline heterostructure via HF etching or SiO_2−SiO_2 inverse opaline

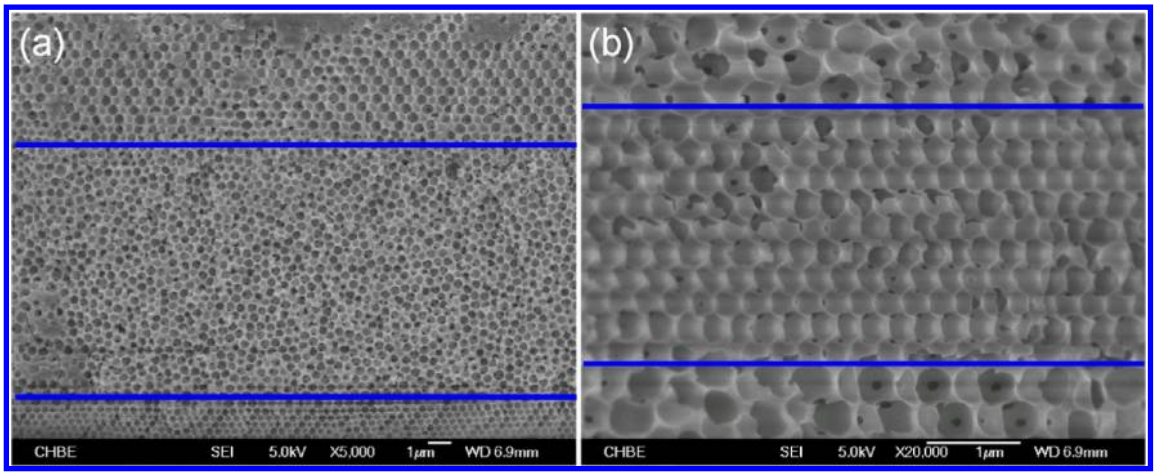

Figure 3. (a) SiO_2 inverse opaline heterostructures fabricated with three different macropore sizes (420−495−560 nm); (b) SiO_2 inverse opaline heterostructures (560−420−560 nm).

heterostructure via calcination. In the following parts, we will focus on the fabrication of inverse opaline heterostructures owing to their wide applications.

3.2. SiO_2−SiO_2 Inverse Opaline Heterostructure. The SEM images of the SiO_2−SiO_2 inverse opaline heterostructure fabricated from 435 nm PS spheres as the top layer and 560 nm PS spheres as the bottom layer are shown in Figure 2. The top view of the inverse opaline film showed a highly ordered structure without cracks at a length scale as large as 100 μm (Figure 2a,b). The inset fast Fourier transform (FFT) in Figure 2a indicates the long-range ordering of the sample. Digital photograph of the films further reveals that uniform heterostructure can be fabricated as large as 2 cm × 1 cm (Figure S1, Supporting Information). The heterostructure can also be fabricated over larger area increasing the volume of the colloidal suspension used while keeping the optimized TEOS-to-PS ratio as a constant. The cross-sectional view in Figure 2c further proves that the film is well ordered and crack-free over a relatively large area. The high-magnification SEM image shows that the SiO_2−SiO_2 heterostructured film has a face-centered-cubic (*fcc*) structure among the coassembled films with (111) plane parallel to the substrate (Figure 2d). To further confirm the effectiveness of this method, we also fabricated SiO_2−SiO_2 inverse opaline heterostructure from opaline heterostructure with 420 nm PS spheres as the top layer and 715 nm PS spheres as the bottom layer (Figure 2e,f and Figure S2, Supporting Information). Both top and cross-sectional views shown in Figure 2e and Figure S2 (Supporting Information) indicate that 3D highly ordered macroporous SiO_2−SiO_2 inverse opaline heterostructure were fabricated over relatively large area without cracks. The interface between two SiO_2 inverse opaline structures with different pore sizes was examined upon partial removal of the upper layer of the inverse opals (Figure 2f). It was found that the top surface of the bottom CC layer was reasonably flat. This flat interface between closely contacted top and bottom CC layers was enabled by two key factors: the original PS/SiO_2 CCs were fabricated in high quality and the bottom CC acted as a flat solid substrate for the growth of the top CC layer.

In addition to SiO_2 inverse opaline heterostructures replicated from two different sizes of PS spheres, our method is also versatile to fabricate more complicated heterostructures. Figure 3a shows SiO_2 inverse opaline heterostructures with three different sizes of pores. Such kind of structure is useful for separation and differential drug release.[42,43] Figure 3b demonstrates a SiO_2 inverse opaline heterostructure embedded with a 3D 420 nm porous layer (560−420−560 nm). It should be pointed out that our method can also be used to embed planar defect in a SiO_2 inverse opaline heterostructure by regulating the colloidal concentration (Figure S3, Supporting Information). Conventionally, planar or 3D defects engineering involves spincoating,[44] LB technique,[45] or an even more complex and expensive method.[46] Our method provides an alternative and cheap method for introducing planar into a SiO_2 inverse opaline heterostructure.

These SEM images indicate that our convective self-assembly method is a promising approach to fabricate crack-free SiO_2−SiO_2 inverse opaline heterostructure films over a relatively large area. In our method, the self-assembly of the CC heterostructure and the associated interfaces between the TEOS sol−gel solution and the colloidal spheres play vital roles in the fabrication of crack-free CC heterostructure films. First, while TEOS itself dissolves well in ethanol, its hydrolyzed form is hydrophilic and is therefore found inside the water-rich emulsion droplets. Hence, the formation of the first layer of CCs benefits the self-assembly of the second layer of CCs, no matter if the interface is hydrophilic or hydrophobic. Second, the interfaces between colloidal spheres and TEOS sol−gel provide sites for the relaxation of tensile stresses generated during the gelation process.[47] Lastly, solvent release during the polycondensation reaction at the interfaces can be controlled and channeled through the interconnected porous network to evaporate at the surface.

The optical reflection spectra of the SiO_2−SiO_2 inverse opaline heterostructure are shown in Figure 4. The SiO_2−SiO_2 inverse opaline heterostructure shows two peaks at ∼550 nm and ∼690 nm (black curve), which are the superposition of SiO_2 replica of PS CCs with sizes of 435 and 560 nm, respectively. The positions of the observed reflectance peaks agree well with 435 nm (red curve) and 560 nm (blue curve) SiO_2 inverse opals though small shifts can be observed. The difference in the intensity of the reflection was caused by the relatively small thickness of the heterostructure films. As reported elsewhere,[22,48] the thicker the CC film, the stronger is the intensity of Bragg diffraction of light.

The positions of the observed reflection peaks can be calculated from the Bragg's law. From Bragg's equation for the (111) planes, the reflection peak can be found as: λ_{max} = (8/

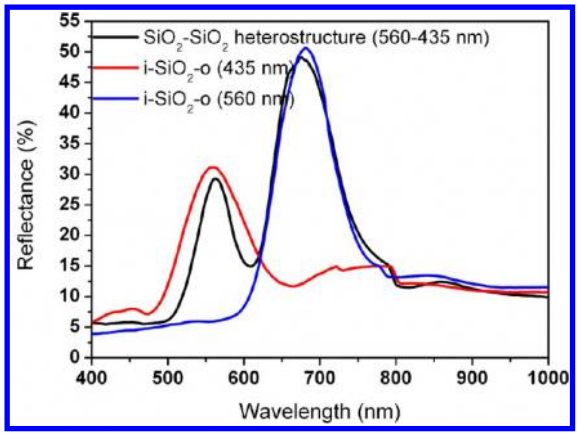

Figure 4. The reflection spectra of a SiO_2−SiO_2 inverse opaline heterostructure comprising 560 nm air spheres at the bottom and 435 nm air spheres at the top. The reflection spectra of a CC composed of inverse SiO_2 opals (i-SiO_2-o) of 560 nm and that of a CC composed of i-SiO_2-o of 435 nm (in diameter) are also included (for comparison).

3)$^{1/2}D(n_{eff}^2 - \sin^2\theta)^{1/2}$, where λ_{max} is the wavelength at the peak position, D is the diameter of PS, n_{eff} is the effective refractive index which can be expressed as $n_{eff}^2 = \Sigma_{i=1}^{N} n_i^2\varphi_i$, n is the refractive index, φ is the volume fraction, subscript i refers to the component, and θ is the angle between the incident light and the reflective surface. In the calculation, we use n_{silica} = 1.455 and n_{air} = 1; for an ideal *fcc* structure, φ= 0.74; thus n_{eff} = 1.136.[11] It should be noted that the shrinkage of the SiO_2 should be taken into account when calculating with the present Bragg's equation. In this case, the shrinkage of the pore is ∼28.7% (the diameters are around 310 and 399 nm, respectively). The calculated λ_{max} from the Bragg's equation are 575 and 740 nm, respectively, which match reasonably well with the measured results when considering that the actual solid volume fraction is often much lower than 26% of a standard closely packed *fcc* structure as a result of dilution of the precursors as well as condensation of the precursors. A filling fraction of ∼20.5% was found for SiO_2 in the resultant heterostructures.

The photonic band structure of the inverse opaline heterostructure along the film stacking direction is a superposition of the photonic band structures of the individual components. By stacking different sized SiO_2 inverse opals or sequentially stacking various inverse opals to form multiple layers, we can fabricate 3D CC heterostructures with an enlarged stop band. Figure 5 shows the reflection spectra of the SiO_2−SiO_2 inverse opaline heterostructure of 715−420, 495−420, and 435−420 nm, respectively. With the decrease of the difference in pore sizes, the two stop bands of the heterostructure change from apparent isolation to close overlap. Such inverse opaline heterostructures with broader stop bands are promising for applications in solar cells,[28] optical filters,[49] and photocatalysis.[50] In addition, CC heterostructure with gradient diameters of macropores may find applications in differential drug release.[42,43]

We also investigated the influence of different stacking sequence on the optical properties of the inverse opaline heterostructures. Figure 6 shows the measured reflection spectra of the SiO_2−SiO_2 inverse opaline heterostructure with two opposite stacking sequences of 420 and 715 nm pore sizes (715−420 and 420−715 nm, respectively). The FESEM image of the 420−715 nm SiO_2−SiO_2 inverse opaline heterostructure

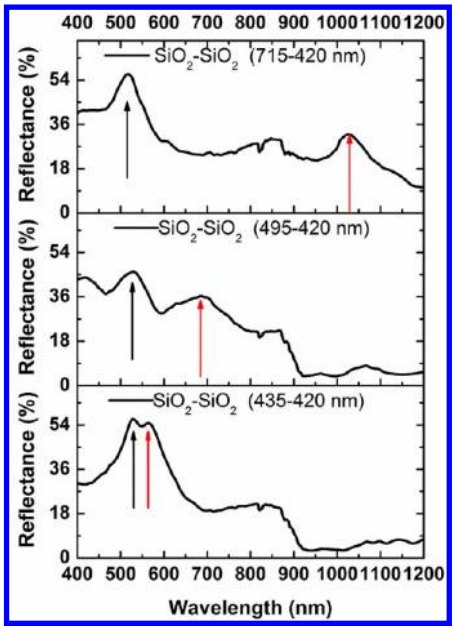

Figure 5. The reflection spectra of SiO_2−SiO_2 inverse opaline heterostructures with varying differences in pore sizes.

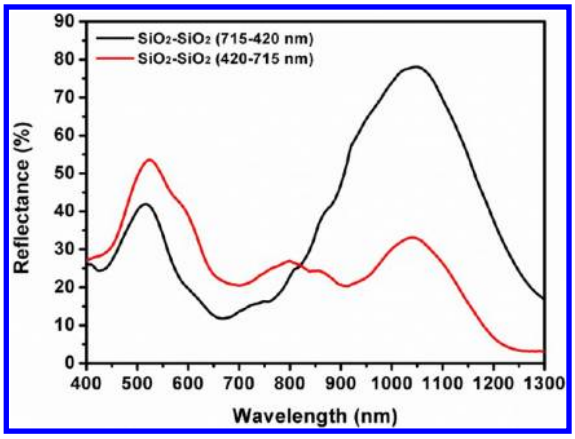

Figure 6. Comparison of the reflection spectra of SiO_2−SiO_2 inverse opaline heterostructures with different stacking sequences (715−420 and 420−715 nm, respectively). The dips centered at ∼820 nm are caused by systematic error due to the detector switching of the spectrophotometer.

is shown in Figure S4, Supporting Information. The spectra of both 715−420 and 420−715 nm SiO_2−SiO_2 inverse opaline heterostructure exhibit two distinctive peaks at ∼500 and ∼1050 nm, respectively. These two peaks correspond to the stop bands of SiO_2 inverse replica of PS CCs with 420 and 715 nm spheres, respectively. From Figure 6, we also note that the stacking sequence does not affect the position of the compositional stop bands.

3.3. SiO_2−TiO_2 Inverse Opaline Heterostructures.

Inverse opaline heterostructure made of two different materials, such as SiO_2−TiO_2, will render one more dimension for tuning the structure properties. However, it is known to be difficult in fabrication owing to the inherent chemical difference between SiO_2 and TiO_2, the surface tension, chemical interaction, and thermodynamics. Here, we demonstrate the fabrication of SiO_2−TiO_2 inverse opaline heterostructures (with 350 nm PS spheres as the bottom layer and 420 nm PS spheres as the top layer) using the same method as that for SiO_2−SiO_2 inverse

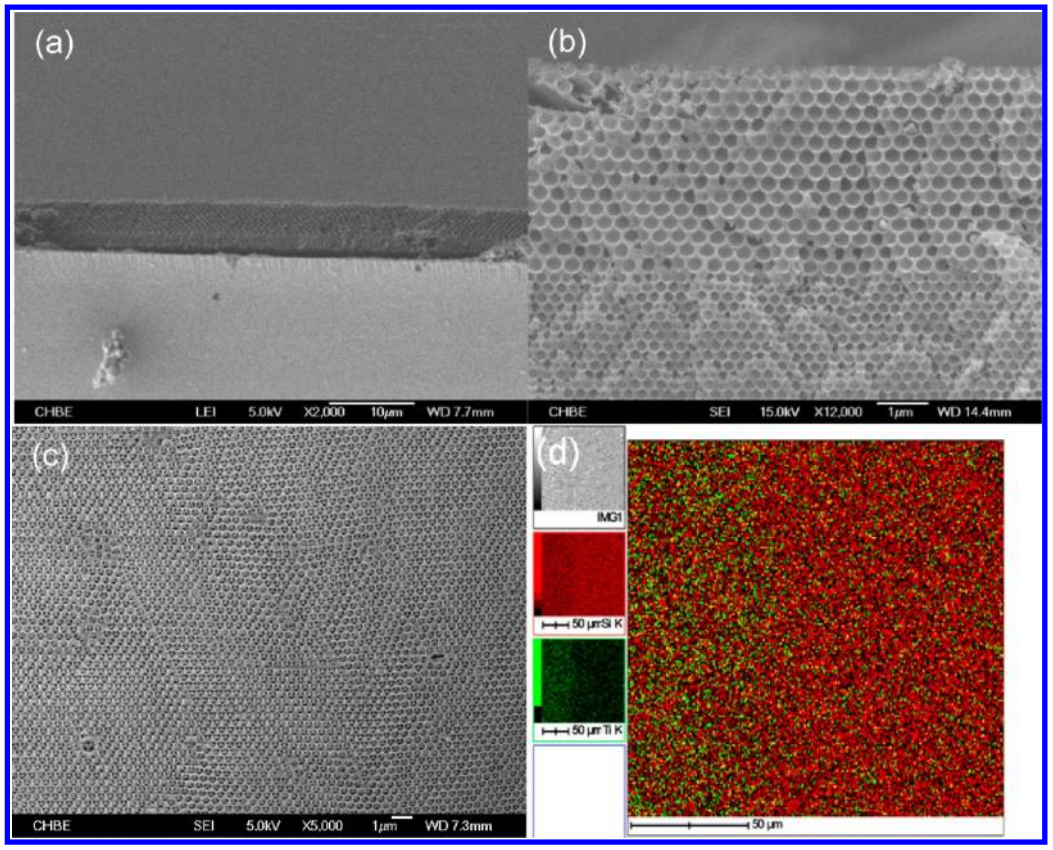

Figure 7. (a,b) Cross section of 350−420 nm SiO_2−TiO_2 inverse opaline heterostructures; (c) top view of 350−420 nm SiO_2−TiO_2 inverse opaline heterostructures; (d) surface mapping of SiO_2−TiO_2 inverse opaline heterostructures by partially removing the upper layer of the samples.

opaline heterostructure. As shown in Figure 7a−c, the pores are well ordered with (111) plane along the substrate. In addition, the SiO_2 layer and TiO_2 layer form seamless junction, which further suggests the effectiveness of our method. Figure 7c shows that relatively large (>50 μm) heterostructure can be produced by this method. Figure 7d shows the surface mapping of the SiO_2−TiO_2 inverse opaline heterostructure by partially removing the upper TiO_2 layer. The red color represents silicon, and the green color represents titanium. As can be seen, the top layer is mainly TiO_2, and the bottom layer is mainly SiO_2. The distributions of silicon and titanium are relatively uniform. In addition, TiO_2−SiO_2 inverse opaline heterostructure can also be fabricated using this method (Figure S5, Supporting Information). It should be mentioned that such SiO_2−TiO_2 and TiO_2−SiO_2 inverse opaline heterostructures are very useful for the fabrication of electrodes of bifacial dye sensitive solar cells. The porous SiO_2 layer can effectively channel the light through the viscous electrolyte and prevents the generation of unwanted back current in a bifacial solar cell and thus effectively improves the photon-energy conversion efficiency.[26,51,52] This heterostructure works at either side illumination and may help bring down the cost of solar energy production. Compared with previously reported approaches,[20,40] our method of fabricating inverse opaline heterostructure is more versatile and more convenient in controlling the quality and kinds of the obtained heterostructure for tailorable applications.

The stop band position of the resultant heterostructure can be predicted using the Bragg's law for the (111) family of the planes too. However, the effective refractive index of the SiO_2−TiO_2 heterostructure is different from the SiO_2−SiO_2 heterostructure. Here, we use $n_{titania}$ = 2.49 and n_{air} = 1 to predict the stop band of the TiO_2 layer; thus n_{eff} = 2.352. A red-shifted Bragg diffraction peak of upper layer of TiO_2 is expected compared to its counterpart of SiO_2 inverse opal films. This is confirmed from the measured reflection spectra (Figure 8), which indicate that the two stop bands of the heterostructure ascribe to that of the compositional individual i-SiO_2-o films and i-TiO_2-o films, respectively. The Bragg refraction peak of top 435 nm i-SiO_2-o film is ∼550 nm (black arrow), while the top 435 nm i-TiO_2-o Bragg refraction peak is ∼770 nm (red arrow).

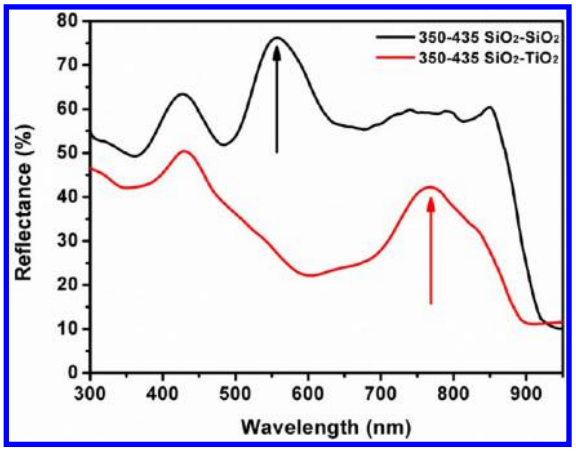

Figure 8. Comparison of the reflection spectra of CC heterostructures fabricated with different materials (350−435 nm SiO_2−SiO_2 and SiO_2−TiO_2).

dx.doi.org/10.1021/am3014482 | ACS Appl. Mater. Interfaces 2012, 4, 5562−5569

4. CONCLUSIONS

In summary, high-quality PS/SiO_2 composite opaline heterostructure and various inverse opaline heterostructure films, including SiO_2−SiO_2 with various pore sizes and SiO_2−TiO_2, were fabricated in a relatively large area using the improved convective self-assembly method. Each compositional inverse opaline structure possesses a close-packed *fcc* structure with the (111) planes oriented parallel to the substrate. The obtained structures possess dual photonic band gaps, which are adjustable through either varying the sizes of the colloidal particles or the materials of the heterostructure. The improved convective self-assembly method can employ a range of organometallic sol−gel and polymer matrix precursors to fabricate other materials, and it represents a simple, low-cost, scalable, and controllable method for fabricating high-quality, chemically tailorable CC heterostructure films for a rich variety of applications in the fields of solar cells, optical filters, differential drug release, photocatalysis, and so forth.

■ ASSOCIATED CONTENT

Ⓢ Supporting Information

Digital photograph of a SiO_2−SiO_2 inverse opaline heterostructure, FESEM images of SiO_2−SiO_2 inverse opaline heterostructure (715−420 nm and 420−715 nm), 715 nm planar defect in a 420 nm inverse opaline structure, and surface mapping of TiO_2−SiO_2 inverse opaline heterostructures (350−420 nm). This material is available free of charge via the Internet at http://pubs.acs.org.

■ AUTHOR INFORMATION

Corresponding Author

*Telephone: (65) 6874 8590 (J.T.); (65) 6516 1071 (X.L.). Fax: (65) 6872 0785 (J.T.); (65) 6779 1936 (X.L.). E-mail: jhteng@imre.a-star.edu.sg (J.T.); chelxm@nus.edu.sg (X.L.).

Notes

The authors declare no competing financial interest.

■ ACKNOWLEDGMENTS

This work was supported by Ministry of Education Singapore under Grant No. R279-000-298-112 and Agency for Science, Technology and Research (A*STAR) under Grant Nos. 0921540099 and 0921540098.

■ REFERENCES

(1) Jiang, P.; Bertone, J. F.; Hwang, K. S.; Colvin, V. L. *Chem. Mater.* **1999**, *11*, 2132−2140.
(2) Vlasov, Y. A.; Bo, X.-Z.; Sturm, J. C.; Norris, D. J. *Nature* **2001**, *414*, 289−293.
(3) Zhu, J.; Li, M.; Rogers, R.; Meyer, W.; Ottewill, R. H.; Crew, S. T. S. S. S.; Russel, W. B.; Chaikin, P. M. *Nature* **1997**, *387*, 883−885.
(4) Míguez, H.; Meseguer, F.; López, C.; Blanco, Á.; Moya, J. S.; Requena, J.; Mifsud, A.; Fornés, V. *Adv. Mater.* **1998**, *10*, 480−483.
(5) Cai, Z.; Teng, J.; Yan, Q.; Zhao, X. S. *Colloids Surf., A* **2012**, *402*, 37−44.
(6) Yan, Q.; Zhou, Z.; Zhao, X. S. *Langmuir* **2005**, *21*, 3158−3164.
(7) Wang, L.; Wan, Y.; Li, Y.; Cai, Z.; Li, H.-L.; Zhao, X. S.; Li, Q. *Langmuir* **2009**, *25*, 6753−6759.
(8) Park, S. H.; Xia, Y. *Langmuir* **1998**, *15*, 266−273.
(9) Gates, B.; Qin, D.; Xia, Y. *Adv. Mater.* **1999**, *11*, 466−469.
(10) Park, S. H.; Qin, D.; Xia, Y. *Adv. Mater.* **1998**, *10*, 1028−1032.
(11) Schroden, R. C.; Al-Daous, M.; Blanford, C. F.; Stein, A. *Chem. Mater.* **2002**, *14*, 3305−3315.
(12) Holgado, M.; Garcia-Santamaria, F.; Blanco, A.; Ibisate, M.; Cintas, A.; Miguez, H.; Serna, C. J.; Molpeceres, C.; Requena, J.; Mifsud, A.; Meseguer, F.; Lopez, C. *Langmuir* **1999**, *15*, 4701−4704.
(13) Meng, X.; Al-Salman, R.; Zhao, J.; Borissenko, N.; Li, Y.; Endres, F. *Angew. Chem., Int. Ed.* **2009**, *48*, 2703−2707.
(14) Rogach, A. L.; Kotov, N. A.; Koktysh, D. S.; Ostrander, J. W.; Ragoisha, G. A. *Chem. Mater.* **2000**, *12*, 2721−2726.
(15) Reculusa, S.; Ravaine, S. *Chem. Mater.* **2003**, *15*, 598−605.
(16) Liu, Y.; Wang, S.; Lee, J. W.; Kotov, N. A. *Chem. Mater.* **2005**, *17*, 4918−4924.
(17) Yan, Q.; Wang, L.; Zhao, X. S. *Adv. Funct. Mater.* **2007**, *17*, 3695−3706.
(18) Arsenault, A.; Fleischhaker, F.; Freymann, G. v.; Kitaev, V.; Miguez, H.; Mihi, A.; Tétreault, N.; Vekris, E.; Manners, I.; Aitchison, S.; Perovic, D.; Ozin, G. A. *Adv. Mater.* **2006**, *18*, 2779−2785.
(19) Stefanou, N.; Yannopapas, V.; Modinos, A. *Comput. Phys. Commun.* **1998**, *113*, 49−77.
(20) Yan, Q.; Zhao, X. S.; Zhou, Z. *J. Cryst. Growth* **2006**, *288*, 205−208.
(21) Jiang, P.; Ostojic, G. N.; Narat, R.; Mittleman, D. M.; Colvin, V. L. *Adv. Mater.* **2001**, *13*, 389−393.
(22) Wong, S.; Kitaev, V.; Ozin, G. A. *J. Am. Chem. Soc.* **2003**, *125*, 15589−15598.
(23) Zhao, Y.; Wostyn, K.; de Schaetzen, G.; Clays, K.; Hellemans, L.; Persoons, A.; Szekeres, M.; Schoonheydt, R. A. *Appl. Phys. Lett.* **2003**, *82*, 3764−3766.
(24) Wostyn, K.; Zhao, Y.; de Schaetzen, G.; Hellemans, L.; Matsuda, N.; Clays, K.; Persoons, A. *Langmuir* **2003**, *19*, 4465−4468.
(25) Rengarajan, R.; Jiang, P.; Larrabee, D. C.; Colvin, V. L.; Mittleman, D. M. *Phys. Rev. B* **2001**, *64*, 205103.
(26) Colodrero, S.; Mihi, A.; Haggman, L.; Ocana, M.; Boschloo, G.; Hagfeldt, A.; Miguez, H. *Adv. Mater.* **2009**, *21*, 764−770.
(27) Seo, Y. G.; Woo, K.; Kim, J.; Lee, H.; Lee, W. *Adv. Funct. Mater.* **2011**, *21*, 3094−3103.
(28) Halaoui, L. I.; Abrams, N. M.; Mallouk, T. E. *J. Phys. Chem. B* **2005**, *109*, 6334−6342.
(29) van Blaaderen, A.; Ruel, R.; Wiltzius, P. *Nature* **1997**, *385*, 321−324.
(30) Massé, P.; Reculusa, S.; Ravaine, S. *Colloids Surf., A* **2006**, *284−285*, 229−233.
(31) Massé, P.; Pouclet, G.; Ravaine, S. *Adv. Mater.* **2008**, *20*, 584−587.
(32) Massé, P.; Ravaine, S. *Chem. Mater.* **2005**, *17*, 4244−4249.
(33) Bardosova, M.; Pemble, M. E.; Povey, I. M.; Tredgold, R. H.; Whitehead, D. E. *Appl. Phys. Lett.* **2006**, *89*, 093116.
(34) Romanov, S. G.; Bardosova, M.; Pemble, M.; Torres, C. M. S. *Appl. Phys. Lett.* **2006**, *89*, 043105.
(35) Baert, K.; Song, K.; Vallee, R. A. L.; Auweraer, M. V. d.; Clays, K. *J. Appl. Phys.* **2006**, *100*, 123112.
(36) Zhang, G.; Wang, D.; Gu, Z.-Z.; Möhwald, H. *Langmuir* **2005**, *21*, 9143−9148.
(37) Yan, L.; Wang, K.; Wu, J.; Ye, L. *J. Phys. Chem. B* **2006**, *110*, 11241−11246.
(38) Yan, L.; Wang, K.; Wu, J.; Ye, L. *Colloids Surf., A* **2007**, *296*, 123−131.
(39) Egen, M.; Voss, R.; Griesebock, B.; Zentel, R.; Romanov, S.; Torres, C. S. *Chem. Mater.* **2003**, *15*, 3786−3792.
(40) Yan, Q.; Teh, L. K.; Shao, Q.; Wong, C. C.; Chiang, Y.-M. *Langmuir* **2008**, *24*, 1796−1800.
(41) Shim, S.-E.; Cha, Y.-J.; Byun, J.-M.; Choe, S. *J. Appl. Polym. Sci.* **1999**, *71*, 2259−2269.
(42) Li, Y. Y.; Cunin, F.; Link, J. R.; Gao, T.; Betts, R. E.; Reiver, S. H.; Chin, V.; Bhatia, S. N.; Sailor, M. J. *Science* **2003**, *299*, 2045−2047.
(43) Cheng, L.; Anglin, E.; Cunin, F.; Kim, D.; Sailor, M. J.; Falkenstein, I.; Tammewar, A.; Freeman, W. R. *Br. J. Ophthalmol.* **2008**, *92*, 705−711.
(44) Wang, L.; Yan, Q.; Zhao, X. S. *Langmuir* **2006**, *22*, 3481−3484.
(45) Griffete, N.; Frederich, H.; Maitre, A.; Chehimi, M. M.; Ravaine, S.; Mangeney, C. *J. Mater. Chem.* **2011**, *21*, 13052−13055.

(46) Tétreault, N.; Mihi, A.; Míguez, H.; Rodríguez, I.; Ozin, G. A.; Meseguer, F.; Kitaev, V. *Adv. Mater.* **2004**, *16*, 346−349.
(47) Cai, Z.; Teng, J.; Wan, Y.; Zhao, X. S. *J. Colloid Interface Sci.* **2012**, *380*, 42−50.
(48) Reynolds, A.; Lopez-Tejeira, F.; Cassagne, D.; Garcia-Vidal, F. J.; Jouanin, C.; Sanchez-Dehesa, J. *Phys. Rev. B* **1999**, *60*, 11422−11426.
(49) Fleischhaker, F.; Arsenault, A. C.; Kitaev, V.; Peiris, F. C.; von Freymann, G.; Manners, I.; Zentel, R.; Ozin, G. A. *J. Am. Chem. Soc.* **2005**, *127*, 9318−9319.
(50) Cai, Z.; Teng, J.; Xiong, Z.; Li, Y.; Li, Q.; Lu, X.; Zhao, X. S. *Langmuir* **2011**, *27*, 5157−5164.
(51) Ito, S.; Zakeeruddin, S. M.; Comte, P.; Liska, P.; Kuang, D.; Gratzel, M. *Nat. Photonics* **2008**, *2*, 693−698.
(52) Bisquert, J. *Nat. Photonics* **2008**, *2*, 648−649.